Anal. Bioanal. Electrochem., Vol. 9, No. 6 , 2017, 762-783

Analytical & Bioanalytical Electrochemistry

2017 by CEE
www.abechem.com

Full Paper

Experimental and DFT Investigation on the Corrosion Inhibition Behavior of Expired Drug Lumerax on Mild Steel in Hydrochloric Acid

Parul Dohare[1], Dheeraj Singh Chauhan[1], Belkheir Hammouti[3], Mumtaz Ahmad Quraishi[1,2*]

[1]*Department of Chemistry, Indian Institute of Technology (Banaras Hindu University), C-8, Ashokpuram Colony, Dafi, Varanasi-221005, India*
[2]*Center of Research Excellence in Corrosion, Research Institute, King Fahd University of Petroleum and Minerals, Dhahran 31261, Saudi Arabia*
[3]*Department of Chemistry, Université Mohammed Premier, Oujda, Morocco*

*Corresponding Author, Tel.: +91-9307025126; Fax: +91- 542-2368428
E-Mail: maquraishi.apc@itbhu.ac.in

Received: 22 May 2017 / Received in revised form: 24 June 2017 / Accepted: 24 July 2017 / Published online: 30 September 2017

Abstract- The present work describes the application of expired drug Lumerax as corrosion inhibitor for mild steel (MS) in 1 M HCl after its expiry date using gravimetric measurements, electrochemical studies and surface analysis. The adsorption of Lumerax on MS surface obeys the Langmuir isotherm. And protection film confirmed by SEM and AFM. Impedance analysis showed that the presence of inhibitor considerably affects the charge transfer resistance and the double layer capacitance of MS surface. Potentiodynamic polarization shows that Lumerax behaves as a mixed type corrosion inhibitor.DFT calculations were used to evaluate the structural, electronic and reactivity parameters of the drug components (Artemether and Lumefantrine) and the theoretical investigation verifies the validity of the use of expired Lumerax drug as a novel and efficient corrosion inhibitor for mild steel.

Keywords– Lumerax, Mild steel, Potentiodynamic polarization, Adsorption, DFT

1. INTRODUCTION

Mild steel (MS) is extensively used in a number of industries owing to its cost effectiveness and excellent mechanical strength. Industrial processes use mineral acids such

as hydrochloric and sulphuric acids for acid pickling and acid descaling etc. to improve oil recovery and removal of scales and salt deposits [1-7]. These acids cause severe corrosion of the oil well/pipe or such structures made up of mild steel [4-7]. In order to control and mitigate the corrosion, the use of organic compounds as corrosion inhibitors is a common protocol [8,9]. Fascinating features of an organic inhibitor are: the presence of heteroatoms (S, N, O, P), π electrons, functional groups, phenyl rings and structural planarity which not only impart the ability to adsorb on a large surface area but enable them to interact with the metal surface via chemical or physical adsorption. Among organic corrosion inhibitors, drugs constitute one of the most sought after types owing to their non-toxicity and environmentally benign nature. Most of the drugs are large organic molecules that contain above structural characteristics in abundance and hence meet the criteria of good corrosion inhibitors. Therefore, the application of drugs as corrosion inhibitors, in recent years has become one of the most actively investigated topics [10-18].

However, there is a major lacuna which restricts the applicability of fresh drugs for corrosion inhibition. Most of the drugs are too expensive in comparison to conventionally used organic inhibitors. Thus, the use of fresh drugs for corrosion inhibition severely puts the cost effectiveness of the method in question. In this context, the expired or unused drugs can provide a fairly reasonable alternative. Here it is important to mention that the date of expiry doesn't mean that a drug or such pharmaceutical compound will lose its potency on or just after a particular point in time. The expiry date in fact, is an assurance from the manufacturer that the said drug will retain at least 90% of its original potency up to that time. In many cases it has been established that under optimal storage condition, some of the drugs can retain their potency and efficacy much longer than the date of expiry. However, physicians or pharmaceutical companies would never recommend the practice of using an expired drug due to professional restrictions and liability concerns.

In most of the cases, people dispose the unused drugs through waste basket or toilet flush through which the drug can be exposed to sunlight, oxygen, moisture or extreme temperature leading to an uncontrolled degradation which can potentially generate toxic waste products [19-21]. The proper disposal of drugs or such pharmaceutical compounds is generally performed by incineration which can contaminate the atmosphere by releasing toxic organics comprising of N, P, S and halogens [22]. Even the controlled degradation procedures are tedious and expensive [23]. Current research activities are focused towards the development of cheap and green corrosion inhibitors [3]. In this regard, the use of expired medicines for corrosion inhibition can fulfil both environmental and economic aspects of green chemistry.

Lumerax (LX) is the trade name of a widely used combination of Artemether and Lumefantrine used as an antimalarial drug for treatment of different kinds of malaria. In the present work, we herein investigate the application of LX in the corrosion inhibition of mild steel in 1 M HCl. The corrosion inhibition behavior was studied using weight loss

measurement, potentiodynamic polarization and electrochemical impedance spectroscopy techniques. In addition, DFT analysis was performed to theoretically estimate the structural aspects of LX significant for corrosion inhibition.

2. EXPERIMENTAL

2.1. Materials and test solutions

The tests were performed on mild steel (MS) strips consisting of about 99.4% Fe by weight. The detailed elemental composition of the MS sample used is reported elsewhere [24]. The MS strips were cut into coupons having dimensions 2.5 cm×2 cm×0.025 cm for use in gravimetric studies. The stock solution of 1 M HCl was prepared by diluting the appropriate amount of 37% HCl, AR grade obtained from Merck.

The LX drug was used as an organic inhibitor in the corrosion studies. The stock solution of the inhibitor was prepared by dissolving the drug in 1 M HCl from which different concentrations were prepared by serial dilution for corrosion testing.

2.2. Gravimetric measurements

The coupons were abraded with emery papers, cleaned, washed with water followed by acetone, dried and weighed accurately as reported earlier [24] according to the NACE Recommended Practice like RP- 0775 and ASTM G-1 & G-4 for weight-loss coupons. The MS coupons were immersed in 1 M HCl in the absence and presence of increasing concentrations of Lumerax (LX) and kept in a thermostat at desired temperature. After an immersion period of 3 h the MS specimens were removed, washed with distilled water followed by acetone wash, dried and then weighed. The corrosion rate (C_R) of the MS specimens in acid solution was determined using equation (1):

$$C_R(mm/y) = \frac{87.6W}{atD} \quad (1)$$

Where, W denotes the average weight loss of MS coupons, a represents the total surface area of one MS coupon, t is the immersion time (3 h) and D is the density of MS in g cm^{-3}.

The corrosion inhibition efficiency ($\eta\%$) was calculated from weight loss values using equation (2):

$$\eta\% = \frac{C_R - {}^{inh}C_R}{C_R} \times 100 \quad (2)$$

Where, C_R and ${}^{inh}C_R$ are the corrosion rates of MS in the absence and presence of the inhibitor, respectively.

Surface coverage (θ) was calculated using equation (3):

$$\theta = \frac{C_R - {}^{inh}C_R}{C_R} \quad (3)$$

2.3. Electrochemical analyses

The electrochemical experiments were carried out using a three electrode assembly in which MS coupon with an exposed area of 1 cm^2 (one sided) was used as a working electrode. A platinum electrode and a saturated calomel electrode (SCE) were used as the auxiliary and the reference electrodes respectively in all the electrochemical experiments. All the potentials are mentioned with respect to the SCE. The electrochemical data were fitted and analyzed using Gamry Echem Analyst 5.0 software. Prior to the electrochemical experiments, the working electrode i.e. MS coupon was allowed to corrode freely in order to establish a steady state open circuit potential (OCP).

The potentiodynamic polarization measurements were carried out by varying the potential from -250 to +250 mV *vs* OCP at a scan rate of 1 mV s^{-1}. Electrochemical Impedance Spectroscopy (EIS) measurements were performed under potentiostatic condition with amplitude of 10 mV peak to peak at the OCP, in the frequency range of 100 kHz to 0.01 Hz. All the electrochemical measurements were conducted at 308 K.

2.4. Surface morphology

The MS specimens were cleaned and immersed in 1 M HCl solution in the absence and presence of optimum concentration of LX. After an immersion period of 3 h, the MS specimens were taken out, washed, dried and used for performing atomic force microscopy (AFM) and scanning electron microscopy (SEM) analyses. The surface analysis through the AFM was carried out using the NT-MDT multimode AFM, Russia, 111 controlled by Solver scanning probe microscope controller. The single beam cantilever with resonance frequency in the range of 240–255 kHz in semi-contact mode having a corresponding spring constant of 11.5 Nm^{-1} having NOVA program was used for image interpretation. The SEM studies were carried out using FEI Quanta 200F scanning electron microscope at a magnification of 500 x.

2.5. Theoretical Study

The theoretical investigations were performed using the Density Functional Theory (DFT) method employing the Becke three-parameter hybrid functional with the Lee-Yang-Paar correlation functional (B3LYP) [25]. The 6-311G(d, p) basis set was utilized for all the calculations. The calculations were performed using Gaussian 09 software for Windows (Revision D.01) [26]. The following quantum chemical parameters were evaluated: energy of

the highest occupied molecular orbital (E_{HOMO}), energy of the lowest unoccupied molecular orbital (E_{LUMO}), energy gap ($\Delta E = E_{LUMO} - E_{HOMO}$), dipole moment ($\mu$), electronegativity ($\chi$), global hardness ($\eta$) and softness ($\sigma$).

3. RESULTS AND DISCUSSION

3.1. Gravimetric measurements

3.1.1. Effect of inhibitor concentration

The influence of the inhibitor concentration on corrosion inhibition efficiency was studied by weight loss measurements for MS in 1 M HCl in the concentration range of 25 mgL^{-1} to100 mgL^{-1}. The results obtained in the absence and presence of different concentrations of LX is shown in Fig. 1a and the corresponding data is listed in Table 1. It can be observed that the corrosion inhibition efficiency increases with increase in the concentration of the inhibitor which indicates the adsorption of the inhibitor molecules on the MS surface. The decrease in weight loss of MS specimens with increase in concentration of LX further supports the above conjecture. At optimum concentration, i.e. 100 mg L^{-1}, the obtained η% was 98.5%.

Table 1. Weight loss data for MS in absence and presence of different concentrations of LX

	Inhibitor Conc (mgL^{-1})	C_R **(mg cm^{-2} h^{-1})**	**Surface coverage (θ)**	η%
Blank	0.0	77.91	---	---
Lumerax	25	16.69	0.786	78.6
	50	8.90	0.885	88.5
	75	5.19	0.933	93.3
	100	1.11	0.985	98.5

3.1.2 Effect of temperature

The influence of temperature on corrosion inhibition efficiency of LX on MS surface was studied at different temperatures from 308 K to 338 K at 100 mgL^{-1}. It can be observed from the graph in Fig. 1b that the η% decreases with increase in temperature. During corrosion, the dissolution of mild steel takes place along with hydrogen evolution in acidic medium. An increase in temperature leads to an increased evolution of hydrogen gas on the cathode which is acting as a sink for the electrons that are being released from the anode. This causes an increased rate of metal dissolution resulting in a higher corrosion rate and comparatively lower inhibition efficiency. Also an elevated temperature results in an increased desorption of the inhibitor molecules from the MS surface which leads to the exposure of a larger surface area of the MS specimen to the acidic medium thereby causing an increased rate of corrosion.

The temperature dependence of corrosion rate can be evaluated from the Arrhenius equation and the Transition state equation as given below [27]:

$$C_R = A\exp\left(\frac{-E_a}{RT}\right) \tag{4}$$

$$C_R = \frac{RT}{Nh}\exp\left(\frac{\Delta S^*}{R}\right)\exp\left(-\frac{\Delta H^*}{RT}\right) \tag{5}$$

Where, E_a is the energy of activation, T is the absolute temperature, A represents the Arrhenius pre-exponential factor and R is the universal gas constant. N is the Avogadro number, h represents the Plank's constant, E_a is the energy of activation, T is the absolute temperature, ΔS^* is the entropy of activation and ΔH^* denotes the enthalpy of activation.

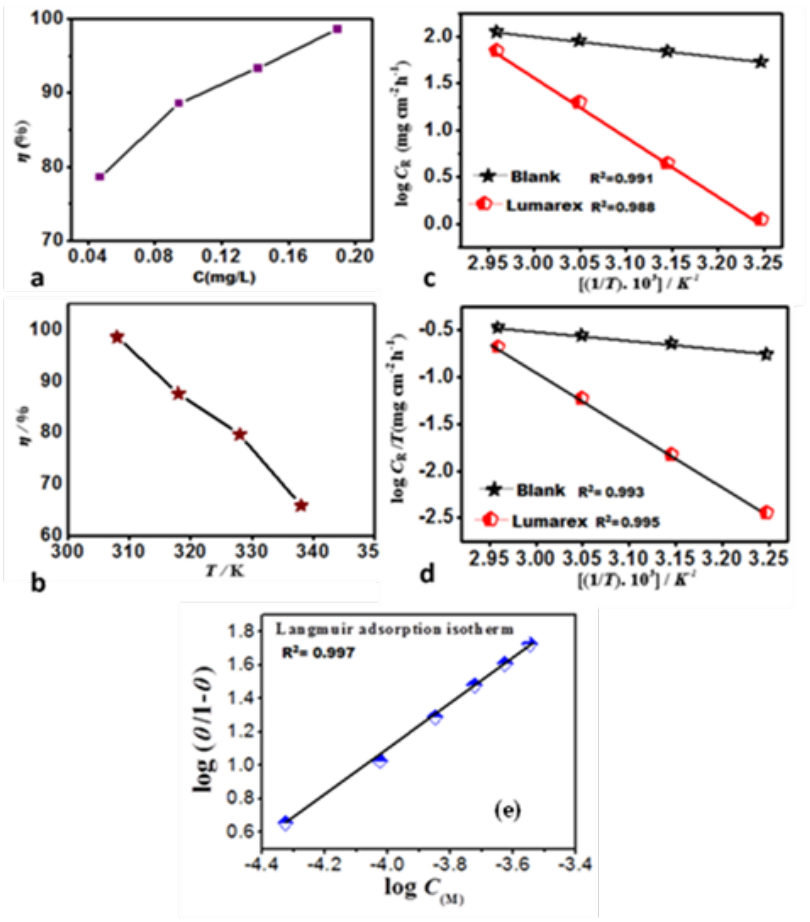

Fig. 1. (a) Variation of the inhibition efficiency (η%) with inhibitor concentration at 308 K; (b) Variation of inhibition efficiency (η%) with solution temperature (308–338 K) at optimum concentration of inhibitor; (c) Arrhenius plots of the corrosion rate (C_R) of MS in 1 M HCl in the absence and presence of 100 mgL^{-1} of LX; (d) Transition-state plots of MS in 1 M HCl in the absence and presence of 100 mgL^{-1} of LX; (e) Langmuir isotherm plot for adsorption of LX on MS surface in 1 M HCl

A graph between log C_R and $1/T$ is known as an Arrhenius plot which gives a straight line having a slope of $E_a / 2.303R$ as shown in Fig. 1c. A plot of log C_R / T *vs* $1/T$ results in a straight line with a slope of $(\Delta H^* / 2.303R$ and an intercept of $[\log (R / Nh) + (\Delta S^* / 2.303R)]$ as shown in Fig. 1d, from where the values of ΔS^* and ΔH^* can be calculated.

The obtained values of E_a and ΔH^* in blank 1 M HCl were 27.90 and 21.65 kJmol^{-1} respectively. In the presence of inhibitor the above values are 93.84 and 86.26 kJmol^{-1} respectively. It can be observed that the values of E_a and ΔH^* in the presence of inhibitor are higher than in its absence. A higher value of E_a in the presence of inhibitor suggests an increase in the thickness of the double layer, which raises the activation energy of the corrosion process [27]. The positive sign of ΔH^* is indicative of a slower dissolution of Fe substrate [28]. The higher values of E_a and ΔH^* in the presence of LX indicate an increase in the energy barrier for the corrosion process. This indicates that with the progressive increase in the concentration of the inhibitor, the corrosion reaction will be driven further to the surface sites categorized by higher values of E_a [29]. Moreover, the ΔS^* in the presence of inhibitor was 60.33 JKmol^{-1} whereas in the absence it was -151.50 Jkmol^{-1}. This increase in the ΔS^* value in the presence of inhibitor is attributed to an increase in randomness on going from the reactants to the activated complex which can result due to the adsorption of the organic inhibitor molecules on the MS surface from the acidic solution. This process can be described as a quasi-substitution between the inhibitor molecules from the aqueous phase and the water molecules present on the surface of MS [30]. The adsorption of inhibitor i.e. LX molecules is accompanied by desorption of water molecules from the surface of MS. Thus, the increase in ΔS^* can be ascribed to an increase in the solvent entropy [31].

3.1.3 Adsorption isotherm

The mode of interaction between inhibitor molecules and the metal surface can be understood by an adsorption isotherm. In the presence of inhibitor, when the corrosion rate is decreased then the adsorption process has a tendency to attain quasi-equilibrium. The nature of the quasi-equilibrium adsorption of inhibitor molecules can be understood using an appropriate adsorption isotherm. The obtained experimental data were tested on several adsorption isotherms among which the Langmuir isotherm was found to provide the best fit as shown by equation (6):

$$\theta / (1-\theta) = K_{ads} C \tag{6}$$

Where, K_{ads} denotes the equilibrium constant of adsorption and C represents the concentration of inhibitor in mgL^{-1}. According to the Langmuir isotherm, a plot of log C *vs* log $\theta / (1-\theta)$ results in a straight line with a regression coefficient close to 1 as shown in

Fig. 1e. The standard free energy of adsorption ΔG^{o}_{ads} and the values of K_{ads} at different temperatures can be computed from equation (7) [32,33]:

$$\Delta G^{o}_{ads} = -RT \ln(1000 K_{ads}) \quad (7)$$

The value 1000 is the concentration of water in solution in gL^{-1}. The calculated values of ΔG^{o}_{ads} and K_{ads} are presented in Table 2. The negative sign indicates that the adsorption of LX on MS surface is a spontaneous process. A value of ΔG^{o}_{ads} around -20 $kJmol^{-1}$ or less negative suggests physical adsorption and around -40 $kJmol^{-1}$ or more negative suggests chemical adsorption [34,35]. In the present study, the calculated values of ΔG^{o}_{ads} range from -27.58 to -31.24 $kJmol^{-1}$ from 308 to 338 K at the optimum concentration (100 mgL^{-1}) of inhibitor. This shows that the mode of adsorption of the inhibitor follows both physical and chemical adsorption.

Table 2. Thermodynamic parameters for the adsorption of LX on mild steel in 1 M HCl at different temperatures

Temp (K)	K_{ads} **(Lg^{-1})**	ΔG^{o}_{ads} **($kJmol^{-1}$)**
308	198.83	-31.24
318	84.25	-30.00
328	90.00	-31.11
338	27.58	-27.58

3.2. Electrochemical analyses

3.2.1 Electrochemical impedance spectroscopy

The electrochemical impedance spectroscopy (EIS) was used to investigate the protective film formed by the adsorbed LX molecules over the surface of MS specimens in 1 M HCl. The Nyquist plots obtained in the absence and presence of varying concentrations of LX are shown in Fig. 2a. The occurrence of single, slightly depressed semicircle loops is indicative of a single time constant. This shows that the electrochemical process is charge transfer controlled and the solid/liquid interface exhibits a non-ideal capacitive behavior [36,37]. Furthermore, the Nyquist plots obtained in the presence of LX are similar to that obtained in the case of blank HCl solution suggesting that the corrosion mechanism has not changed after the introduction of inhibitor in the medium [37]. By applying the equivalent circuit shown in Fig. 2b, the different EIS parameters such as, *n* (phase shift), R_s (solution resistance), C_{dl} (double layer capacitance) and R_p (polarization resistance) were calculated and are shown in

Table 3. Usually the difference between the Z_{real} values at the high and low frequencies is termed as R_{ct}. In the present case, the R_p represents the polarization resistance which consists of the charge transfer resistance (R_{ct}), double layer resistance (R_d), film resistance (R_f) and the resistance due to the accumulation of adsorbed molecules (R_a) [24-26].

An increase in the diameter of the capacitive loops with increase in the concentration of the inhibitor suggests that the LX acts as an efficient corrosion inhibitor for MS. The inhibitor molecules get adsorbed on the MS surface and block the active sites available for corrosion thereby causing an increase in the R_p values which is associated with the mitigation of corrosion. The inhibition efficiency can be calculated as follows,

$$\eta\% = \frac{R_{p(inh)} - R_p}{R_{p(inh)}} \times 100 \tag{8}$$

Where, $R_{p(inh)}$ and R_p are the values of polarization resistance in the absence and the presence of inhibitor in 1 M HCl respectively. The inhibition efficiency obtained in the presence of LX at 100 mgL^{-1} is 97.6%. The Equivalent circuit model shown in Fig. 4b was used to analyze the Nyquist plots and it consists of R_s and CPE (constant-phase element) parallel to the R_p [36,37]. In order to define the capacitance of the depressed Nyquist semicircles, in the place of a pure capacitor, a non-ideal capacitor is introduced in the circuit (defined as constant phase element: CPE) whose impedance is given by [36-38]:

$$Z_{CPE} = Y_o^{-1}(j\omega)^{-n} \tag{9}$$

Where, Z_{CPE} is the impedance of CPE, Y_o is the CPE coefficient (reciprocal of impedance and also known as admittance) and ω is the angular frequency given by $\omega = 2\pi f$ (having units in rad sec^{-1}). According to the above equation, the phase angle of the CPE impedance becomes independent of frequency having a value of $(-n\pi/2)$ degrees. Hence the CPE is called the “constant phase element". The numerical value of n is given by the slope of the linear region of the Bode plot. When the value of n reaches unity, the equation (9) becomes,

$$\frac{1}{Z_{CPE}} = Y_o j\omega = j\omega C \tag{10}$$

Thus, the CPE behaves as a capacitor when n is close to 1 [39,40]. The double layer capacitance (C_{dl}) can be evaluated as follows:

$$C_{dl} = \frac{Y_o \omega^{n-1}}{\sin(n(\pi/2))} \tag{11}$$

Where, ω is given by $\omega_{\max} = 2\pi f_{\max}$ at which the imaginary part of the impedance $(-Z_{im})$ is maximum and other symbols are as defined above.

The value of n and hence the CPE are controlled by heterogeneities occurring at the microscopic level at the metal/ electrolyte interface. Thus, the behavior of CPE can be thought of as having a geometric origin and n is also defined as the roughness coefficient. Although the CPE is introduced only to fit the impedance data, an increase in the value of n can be associated with an increase in the surface homogeneity. Thus, the CPE resembles a resistor when n =0 and an inductor when n = -1 [40].

The Bode and phase angle plots for MS in 1 M HCl in the absence and presence of varying concentrations of inhibitor are shown in Fig. 2c. Thus, in the present case, a low value of n in blank solution suggests a surface inhomogeneity arising due to the roughening of metal surface and/or formation of corrosion products [40]. However, in the presence of inhibitor close to the optimum concentration, the values of n are considerably higher and are tending to unity that is towards ideal capacitive behavior [39]. In the presence of LX, an increase in the low frequency impedance modulus takes place which is an indicative of the adsorption of inhibitor molecules and an improvement in the corrosion resistance of MS surface.

Moreover, it can be observed from the Table 3 that an increase in the concentration of inhibitors, in addition to causing an increase in R_p, also causes a corresponding decrease in the double layer capacitance. The inhibitor molecules get adsorbed on the MS surface by displacing the water molecules and other adsorbed ions and form a protective film on the electrode surface. The thickness of this film increases with increase in the concentration of the inhibitor, since more and more inhibitor molecules get adsorbed on the metal surface leading to a gradual decrease in C_{dl} values as shown in Table 3.

The thickness of the protective layer of inhibitor δ_{org} can be related to the C_{dl} as follows:

$$C_{dl} = \frac{\varepsilon_0 \varepsilon_r}{\delta_{org}} \tag{12}$$

Where, ε_0 is the vacuum dielectric constant and ε_r is the relative dielectric constant.

Table 3. Electrochemical impedance parameters and corresponding corrosion inhibition efficiency in the absence and presence of different concentrations of LX

	Inhibitor conc. (ppm)	$R_s(\Omega)$	$R_{ct}(\Omega cm^2)$	n	$Y_o(\mu F cm^{-2})$	$C_{dl}(\mu F cm^{-2})$	$\eta\%$
Blank		0.80	9.0	0.80	481.10	134.2	---
Lumerax	25	0.75	105.15	0.79	225.60	81.74	81.4
	50	0.97	333.12	0.73	51.50	13.4	91.2
	75	0.73	495.17	0.80	52.14	17.9	93.8
	100	0.76	764.73	0.89	31.10	17.5	97.6

The decrease in the values of C_{dl} might result from the lowering of local dielectric constant or from the increase in thickness of the electrical double layer, which suggests that the inhibitor molecules function by adsorbing at the metal/solution interface. Thus, the observed decrease in the C_{dl} values is caused by the gradual replacement of water molecules by the adsorption of inhibitor molecules on the metal surface, which decreases the metal dissolution.

The phase angle value for the MS surface in the absence of LX is -40.74° which shows considerable deviation from the value for an ideal capacitor i.e. -90° due to corrosive attack of acid solution. However, in the presence of increasing concentrations of LX, the phase angle values show a successive increase and approach towards -90°. This indicates a considerably improved capacitive performance of the MS surface in the presence of inhibitor. This suggests that the adsorbed inhibitor molecules form a protective film on the surface of MS thereby improving the surface homogeneity and in turn better capacitive behavior [41].

3.2.2. Potentiodynamic polarization study

The polarization curves recorded for the MS coupons in the absence and presence of varying concentrations of LX in 1 M HCl are shown in Fig. 2d. To obtain a deeper insight on the corrosion inhibition process, the different electrochemical parameters, i.e., corrosion potential (E_{corr}), corrosion current density (i_{corr}), anodic and cathodic slopes (β_a and β_c) and inhibition efficiency ($\eta\%$) values were determined from the corresponding Tafel plots and the obtained data are represented in Table 4. The inhibition efficiencies can be calculated from i_{corr} values from the equation below,

$$\eta\% = \frac{i_{\text{corr}} - i_{\text{corr(inh)}}}{i_{\text{corr}}} \times 100 \tag{13}$$

Where, i_{corr} and $i_{corr(inh)}$ are the corrosion current densities of MS in 1 M HCl in the absence and presence of inhibitor. It can be observed from Fig. 2d that in the presence of the inhibitors, both the anodic and cathodic curves shift towards lower current density, indicating the suppression of both the cathodic as well as anodic reaction as compared to blank. This decrease in the corrosion current density in presence of inhibitor suggests that the rate of electrochemical reaction was reduced due to the formation of a protective barrier layer of inhibitor molecules over the MS surface [42]. From Table 4, it can be observed that the cathodic Tafel slope (β_c) values are significantly greater than that of the anodic Tafel slope (β_a) values. This indicates that the influence of inhibitor on the kinetics of hydrogen evolution is more prominent than that on Fe dissolution [43]. Also, the β_c values in the presence of inhibitor are considerably higher than in the blank solution suggesting a change

in the mechanism of hydrogen evolution [44,45]. Further, a negative shift in the E_{corr} values indicates that the inhibitor has a more significant effect on the cathodic process than on the anodic process. Although, this shift is not considerable enough for the inhibitor to be classified as cathodic type and indicates a mixed type inhibition behavior.

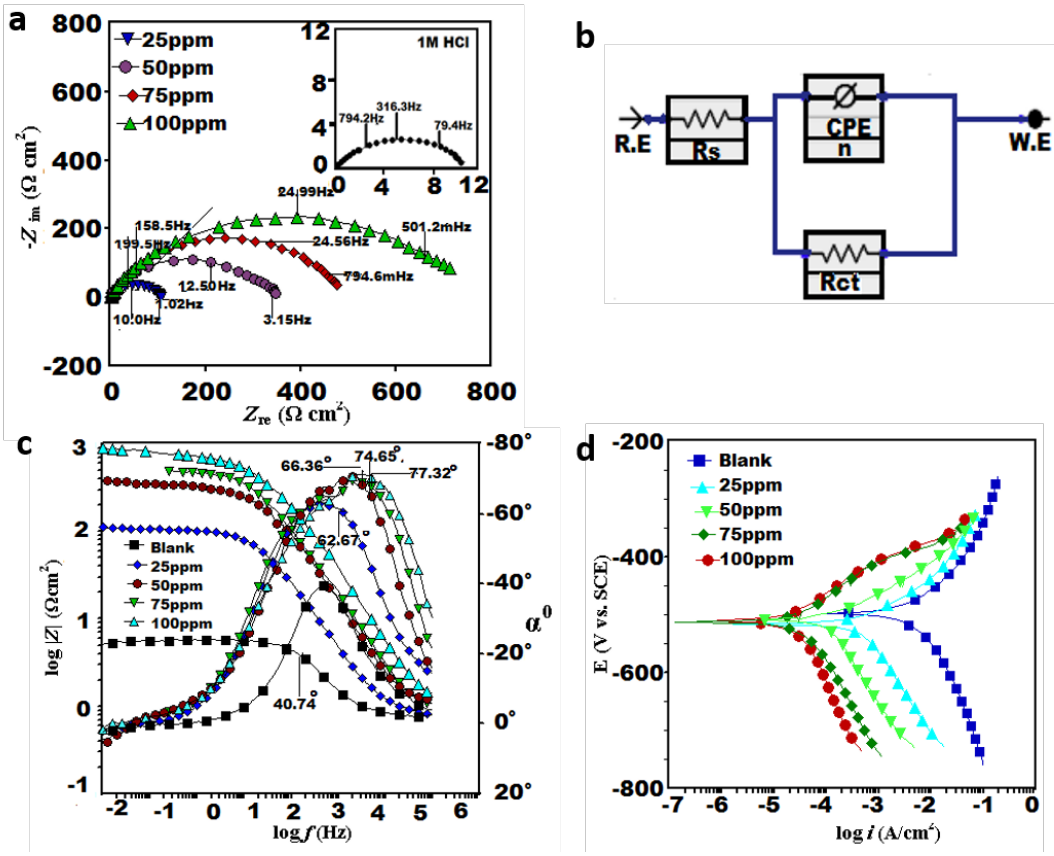

Fig. 2. (a) Nyquist plots for MS surface in 1 M HCl in the absence (inset) and presence of different concentrations of LX at 308 K; (b) Equivalent circuit model used to fit the EIS data; (c) Bode (log f *vs* log |Z|) and phase angle (log f *vs* α) plots of impendence spectra for MS in 1 M HCl in the absence and presence of different concentrations of ETr at 308 K; (d)Polarization curves for MS in the absence and presence of different concentrations of ETr

Table 4. Polarization data for MS in the absence and presence of different concentrations of LX

Inhibitor conc. (ppm)	E_{corr} **(mV vs.SCE)**	β_a **(mV/dec)**	β_c **(mV/dec)**	I_{corr} **(µA/ cm^2)**	η%
Blank	-443	85.7	100.8	892	--
Lumerax					
25	-513	103.1	145.7	150	83.1
50	-512	83.9	170.3	95	89.3
75	-506	85.5	166.6	62	92.7
100	-501	95.2	171.1	42	95.2

3.3. Surface morphology

3.3.1. Structural characterization of inhibitor

As mentioned earlier, the expired drugs promise to be a potential candidate to cut down the large expenses on fresh drugs and the synthetic organic inhibitors. However, a major issue in this case is the possible degradation/ decomposition of the active constituents of the drug due to unfavorable exposure to moisture, temperature, and sunlight etc. arising out of poor storage conditions. Therefore, the FTIR analysis of fresh and expired LX was carried out and a comparison was made to understand whether there was a significant difference in structure after the expiration date. The results shown in Fig. 3(a) indicate that even after the expiration date, there is no major discernible difference between the expired and fresh LX. The sp^3 C-H stretch of Artemether can be observed near ~2950 cm^{-1}. The –C-O peak can be seen at ~1300 cm^{-1}. The peak for –OH from Lumefantrine can be observed at ~3400 cm^{-1}. The peak for aromatic -C-Cl can be seen at ~900 cm^{-1}. The C-N stretch can be visualized at 1080 cm^{-1}. Thus, this result validates the applicability of the expired LX drug as corrosion inhibitor for mild steel in acidic medium.

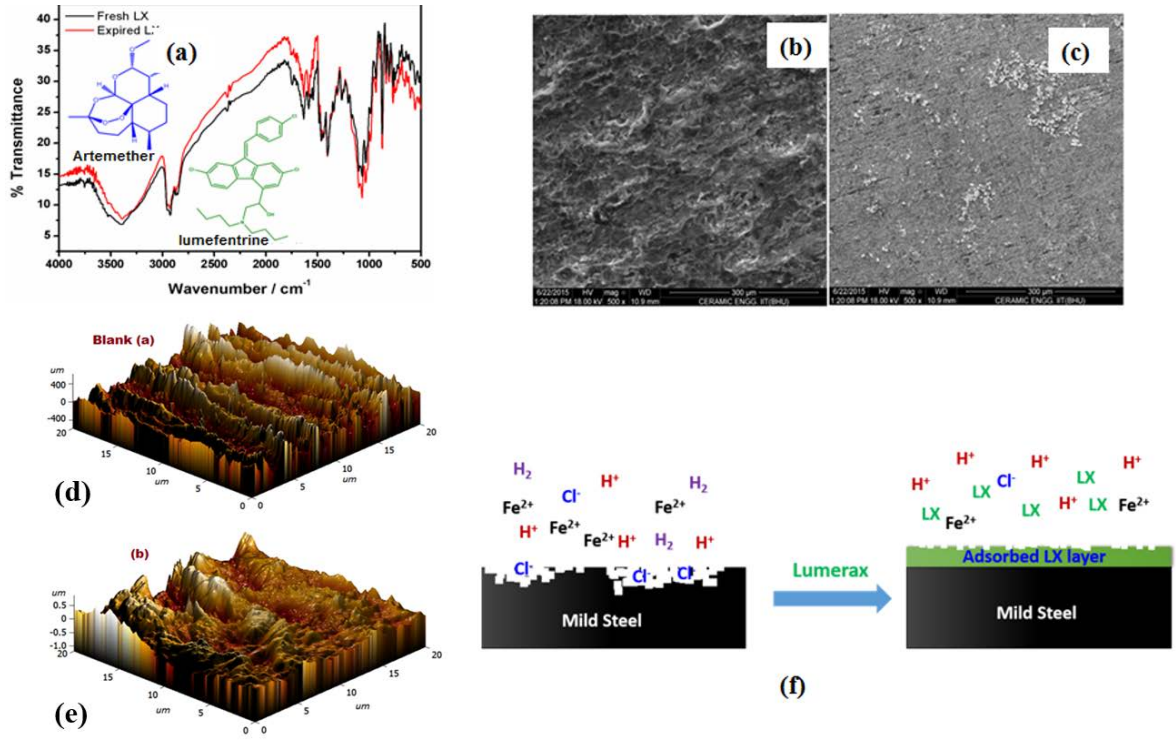

Fig. 3. (a) FTIR of fresh and expired Lumerax drugs, SEM micrographs of MS surface; (b) in 1 M HCl; (c) in 1 M HCl with 100 mgL^{-1} of LX. AFM images of MS surface; (d) in 1 M HCl; (e) in 1 M HCl with 100 mgL^{-1} of LX; (f) Schematic of possible modes of adsorption of ETr on mild steel surface and its corrosion inhibition behavior

3.3.2. Scanning electron microscopy

The SEM images of the MS specimens after 3 h immersion period in 1 M HCl in the absence and presence of optimum concentration of LX are shown in Fig. 3(b-c). The image of the MS specimen which was immersed in blank HCl solution shows a highly rough and corroded surface due to the corrosive attack of acid. On the other hand, the image of MS specimen which was immersed in the presence of inhibitor shows a significantly smoother surface with lesser pits and cracks which suggests that the inhibitor formed a protective film over the MS surface which protected it from corrosion in the acidic medium.

3.3.3. Atomic force microscopy

The AFM images of the MS specimens immersed in 1 M HCl without and with optimum concentration of inhibitor after duration of 3 h are shown in Fig. 3(d-f). The MS surface was found severely corroded and damaged in the blank solution i.e. in the absence of inhibitor as shown in Fig. 3 (d). A number of deep striations can be visualized which can be associated with polishing scratches. The surface topography of the MS specimen in the presence of inhibitor was significantly improved as depicted in Fig. 3(e). The smoothness of the MS surface in the presence of inhibitor molecules is attributed to retardation in corrosion processes. Thus, the surface morphology substantiates the results obtained by electrochemical measurements discussed above. A schematic of the adsorption and corrosion inhibition action of LX is illustrated in Fig. 3(f).

3.4. Theoretical investigation

Computational analyses are frequently applied for predicting structure-activity relationships of pharmaceutically active compounds in the areas of drug design and drug discovery. In the domains of corrosion inhibition, one such method is Density Functional Theory (DFT) which has had a huge impact on the development of quantum electrochemistry [46]. The DFT calculation is carried out in order to obtain theoretical parameters such as charge distribution, dipole moment and frontier orbital electron density for designing novel and high performance corrosion inhibitors [10,47,48]. From the detailed experimental results, it is obvious that the present drug LX acts as an efficient inhibitor against corrosion of mild steel in 1 M HCl. As mentioned earlier, LX is a combination of two drug components i.e., Artemether (ART) and Lumefantrine (LUM). Hence, it is important to find out which of the two drugs i.e. ART or LUM has a more prominent influence on the corrosion inhibition behavior. Therefore, the DFT analysis was performed to study the structural properties of the two drug components.

The optimized molecular structures of ART and LUM are shown in Fig. 4(a-b). It can be observed that ART shows a non-planar and considerably distorted structure. On the other

hand, LUM exhibits a highly planar and widely stretched arrangement which is a major criteria for better adsorption and corrosion inhibition [49]. The Mulliken charge distribution and the HOMO populations are determined in order to predict the possible adsorption centers present in an inhibitor molecule [50,51]. In general, the more negatively charged hetero atoms/regions with major distribution of HOMO are the most probable sites of adsorption [52]. The HOMO electron density surface of a molecule is associated with the sites that are more likely to donate electrons. Thus, a higher HOMO energy indicates the ability of an inhibitor to donate electrons to d-orbitals of the metal. The LUMO electron density surface is associated with a tendency of electron acceptance. Thus an inhibitor molecule with a lower LUMO energy can easily accept electrons from the filled orbitals of metal.

The HOMO and LUMO electron density distributions of ART and LUM are shown in Fig. 4 (c-f). The HOMO of ART is spread around the closely arranged oxygen atoms while the other oxygen present in the side chain doesn't contribute to HOMO. The LUMO is distributed over the aliphatic rings of ART. The HOMO of LUM is mainly centered on the heteroatoms i.e. tertiary amino and the hydroxyl groups along with the cyclopentadiene ring and the adjacent phenyl ring suggesting that these are the major centers for electron donation. The LUMO is widely distributed over all the three phenyl rings and the five membered rings. The calculated quantum chemical parameters are listed in Table 5. The LUM has a higher E_{HOMO} value than ART and thus it exhibits a higher tendency to donate electrons to Fe. The trend in E_{LUMO} values however, doesn't agree with that obtained in the E_{HOMO} values. However, the energy gap i.e., ΔE is lower in case of LUM which supports its greater inclination to get adsorbed on the MS surface.

According to Koopman's theorem [53-56], the frontier orbital energies can be given by:

$$-E_{HOMO} = I \tag{14}$$

$$-E_{LUMO} = A \tag{15}$$

Where, I is the ionization potential, and A is the electron affinity of the chemical system. The absolute electronegativity (χ), is a measure of the electron attraction ability by a group of atoms toward itself and it can be evaluated as follows:

$$\chi = \frac{1}{2}(I + A) = -\frac{1}{2}(E_{HOMO} + E_{LUMO}) \tag{16}$$

The global electronegativity indicates the extent to which a molecule can retain its electrons. The higher value of χ can be associated with a lower tendency of electron donation by an inhibitor molecule and vice versa. From the data of the χ values for ART and LUM shown in Table 5, it is clear that $\chi_{ART} > \chi_{LUM}$ which suggests that LUM has a higher ability of donating electrons to an electrophilic center such as Fe surface having an accumulation of positive charges [3].

The global hardness (η) is a parameter measuring the resistance in transfer of charge and its inverse is the global softness (σ) [56,57]. The hardness and softness can be related with the HOMO and LUMO energy values as follows:

$$\eta = \frac{1}{2}(I - A) = -\frac{1}{2}(E_{HOMO} - E_{LUMO}) \quad (17)$$

$$\sigma = \frac{1}{\eta} \quad (18)$$

The results shown in Table 5 depict a lower value of hardness and hence a higher softness of LUM in comparison to ART. Earlier, Pearson has described that the hard molecules have a large HOMO-LUMO gap and soft molecules have a small HOMO-LUMO gap [54,56]. Thus, these data correlate well with those of the trend in the energy gap values shown above. The soft molecules are more reactive than the hard ones because they can easily offer electrons to an acceptor. Bulk metals are soft acids and hence soft base inhibitors are most effective for inhibition of acidic corrosion of these metals according to HSAB principle. In general, the molecule having a lower value of global hardness is likely to exhibit higher inhibition efficiency [58,59].

Gomez *et al* have proposed that in the cases where the charge is being transferred to a molecule as well as a back-donation of electrons from the molecule are taking place, the change in energy is directly proportional to the hardness of the molecule [59] and is given by the expression,

$$\Delta E_{back-donation} = -\frac{\eta}{4} \quad (19)$$

In the above equation, since the η>0, this makes the $\Delta E_{back-donation} < 0$. This condition means that the charge transfers to a molecule and the back-donation of electrons from the molecule are energetically favorable. It can be observed from Table 5 that LUM has a higher energy of back-donation than ART.

The dipole moment (μ) was also evaluated with DFT although there are disputed views on the correlation between the dipole moment and the corrosion inhibition efficiency [3,38,61]. On one hand, it is believed that an increase in the dipole moment results in a decrease in inhibition efficiency because the low values of dipole moment will favor accumulation of the inhibitor molecules in the surface layer, whereas the other view states that a high dipole moment will lead to an increment in the inhibition efficiency due to increased dipole−dipole interactions between the inhibitor molecules and the metal surface. The obtained dipole moment values are in the order LUM>ART and thus, support the opinion that a higher dipole moment will result in a higher inhibition efficiency.

Table 5. Calculated quantum chemical parameters of neutral and protonated Artemether (ART) and Lumefantrine (LUM)

Component	E_{HOMO}	E_{LUMO}	ΔE	χ	η	σ	$\Delta E_{back-donation}$	μ
ART	-3.92	-2.63	1.28	3.28	0.64	1.56	-0.16	8.10
LUM	-2.52	-1.91	0.61	2.21	0.30	3.33	-0.08	10.13

All energy values are in eV; σ is in eV^{-1}; μ is in Debye

The theoretical investigation elucidates that the component LUM present in LX has a prominent influence on the corrosion inhibition behavior. Here it is important to note that the LX is sold by different trade names such as Lumerax-20, Lumerax-40, Lumerax-60, Lumerax-80 etc. having different dosage amounts to meet the requirements of patients of different age and health condition.

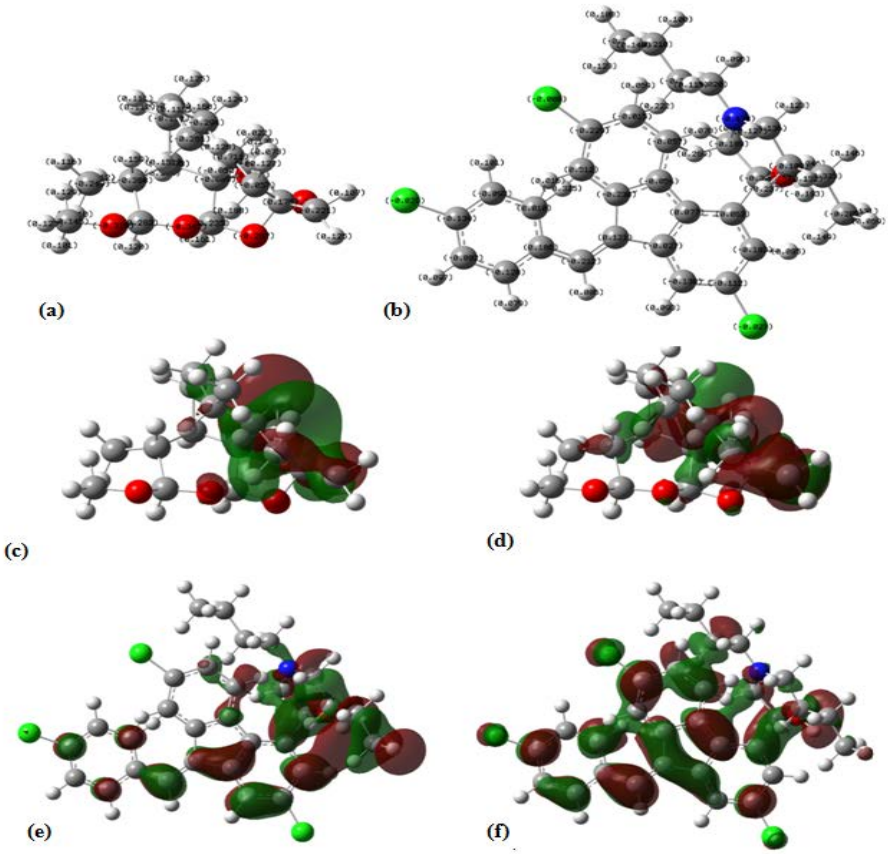

Fig. 4 Optimized structures of (a) Artemether and (b) Lumefantrine showing Mullikan charges. Frontier molecular orbital electron density distribution of Artemether (c) HOMO (d) LUMO; and Lumefantrine (e) HOMO (f) LUMO

However, the weight ratio of ART: LUM is 1:6 which is always kept constant in LX. A typical example is Lumerax-80 which was used in the present work that contains 80 mg ART and 480 mg LUM. Since the proportion of LUM is six times to that of ART, therefore it is more likely to govern the corrosion inhibition behavior of the mixed product i.e. LX. In other words, this also suggests that the present antimalarial drug LX is widely used among patients from a variety of age groups and disease conditions and is very likely to enter and contaminate the environment. This justifies the utilization of expired LX in corrosion inhibition.

Table 6 shows a comparative data on the corrosion inhibition performance of some of the earlier reported expired drugs along with that of the LX. It can be observed from the Table 6 that LX shows considerably significant corrosion inhibition efficiency compared to other expired drugs. Therefore, it can be seen that the present expired drug i.e. LX can be utilized for corrosion inhibition application with promising results. It is obvious from the present work that the use of expired drugs is a significantly cost effective means to control corrosion. Furthermore, this study purports a green alternative to otherwise costly and cumbersome disposal and degradation procedure of expired drugs which are a major source of environmental nuisance.

Table 6. Different expired drugs and their inhibition efficiency in IM HCl on mild steel

Drug	**Test medium**	**Metallic surface**	η%	**Ref.**
Carbamazepine	0.1 M H_2SO_4	Carbon steel	90	[22]
Paracetamol	0.25 M Acetic acid-0.25 M sodium acetate buffer	Carbon steel	85	[22]
Voltaren	1 M HCl	Aluminium	89.7	[62]
1- Phenytoin	1 M HCl	Carbon steel	79.1	[63]
Amlodipine Besylate	1 M HCl	Low Carbon steel	94.3	[64]
Asthalin	1 M HCl	Mild steel	94.76	[65]
Ranitidine	1 M HCl	Mild steel	90.0	[66]
Amlodipine Besylate	1 M HCl	Low Carbon steel	83.5	[67]
Lupicof	1 M HCl	Mild steel	70.86	[68]
2-(2, 6-dichloranilino) phenyl acetic acid	1 M HCl	Mild steel	87.5	[69]
Lumerax	**1 M HCl**	**Mild steel**	**95.30**	**Present work**

4. CONCLUSIONS

Lumerax (LX) acted as a good corrosion inhibitor for mild steel in 1 M HCl and the inhibition process was found to depend on the concentration of the inhibitor. An increase in

the concentration of the inhibitor led to an increased corrosion inhibition efficiency, whereas an increase in temperature was found to have a negative influence on the inhibition efficiency. The adsorption mode of inhibitor on mild steel surface follows Langmuir isotherm. The values of K_{ads} and ΔG^{o}_{ads} together with the reduced rate of corrosion in the presence of inhibitor indicated its strong adsorption on the mild steel surface. EIS spectra exhibited a single time constant and showed that with an increase in the inhibitor concentration, the charge transfer resistance (R_p) increased while the double layer capacitance (C_{dl}) decreased. Polarization curves pointed out that the inhibitor shows a mixed type behavior and suppresses both the anodic and cathodic reactions while showing a predominant influence on the cathodic process. The theoretical calculations provided a strong support for the obtained experimental results.

Acknowledgements

Parul Dohare is thankful to the Ministry of Human Resource Development (MHRD), New Delhi, India for providing financial assistance. Authors are thankful to Mr. M. Prakash, Mr. L. Devender Nayak, for his valuable assistance and, Mr. N. Gupta for his generous inputs and suggestions.

REFERENCES

[1] A. S. Fouda, and A. S. Ellithy, Corros. Sci. 51 (2009) 868.
[2] M. Behpour, S. M. Ghoreishi, N. Soltani, M. Salavati-Niasari, M. Hamadanian, and A. Gandomi, Corros. Sci. 50 (2008) 2172.
[3] P. Dohare, K. R. Ansari, M. A. Quraishi, and I. B. Obot, J. Indust. Eng. Chem. 52 (2017) 197.
[4] M. Faustin, A. Maciuk, P. Salvin, C. Roos, and M. Lebrini, Corros. Sci. 92 (2015) 287.
[5] N. Esmaeili, J. Neshati, and I. Yavari, J. Ind. Eng. Chem. 22 (2015) 159.
[6] M. H. Abd, and E. l. Lateef, Corros. Sci. 92 (2015) 104.
[7] P. Singh, E. E. Ebenso, L. O. Olasunkanmi, I. B. Obot, and M. A. Quraishi, J. Phys. Chem. C 120 (2016) 3408.
[8] A. Döner, R. Solmaz, M. Özcan, and G. Kardas, Corros. Sci. 53 (2011) 2902.
[9] P. M. Dasami, K. Parameswari, and S. Chitra, Measurement 69 (2015) 195.
[10] G. Gece, Corros. Sci. 53 (2011) 3873.
[11] I. B. Obot, E. E. Ebenso, and M. Kabanda, J. Environ. Chem. Eng. 1 (2013) 431.
[12] S. K. Shukla, and M. A. Quraishi, Corros. Sci. 51 (2009) 1007.
[13] S. K. Shukla, A. K. Singh, I. Ahamad, and M. A. Quraishi, Mater. Lett. 63 (2009) 819.
[14] S. K. Shukla, and M. A. Quraishi, Mater. Chem. Phy. 120 (2010) 142.
[15] A. K. Singh, and M. A. Quraishi, Corros. Sci. 52 (2010) 152.

[16] I Ahamad, R. Prasad, and M. A. Quraishi, J. Solid. State. Electrochem. 14 (2010) 2095.
[17] I. Ahamad, R. Prasad, and M. A. Quraishi, Corros. Sci. 52 (2010) 651.
[18] I. Ahamad, R. Prasad, and M. A. Quraishi, Corros. Sci. 52 (2010) 3033.
[19] M. Kotchen, J. Kallaos, K. Wheeler, C. Wong, and M. Zahller, J. Environ. Manage. 90 (2009) 1476.
[20] S. K. Khetan, and T. J. Collins, Chem. Rev. 107 (2007) 2319.
[21] I. S. Ruhoy, and C. G. Daughton., Sci. Total Environ. 388 (2007) 137.
[22] N. Vaszilcsin, V. Ordodi, and A. Borza, Int. J. Pharm. 431 (2012) 241.
[23] K. J. Ottmar, L. M. Colosi, and J. A. Smith, Chemosphere 88 (2012) 1184.
[24] C. Verma, L. O. Olasunkanmi, I. B. Obot, E. E. Ebenso, and M. A. Quraishi RSC Adv. 6 (2016) 53933.
[25] A. D. Becke, J. Chem. Phys. 98 (1993) 5648.
[26] Gaussian 09, Revision D.01, M. J. Frisch, G. W. Trucks, H. B. Schlegel, G. E. Scuseria, M. A. Robb, J. R. Cheeseman, G. Scalmani, V. Barone, B. Mennucci, G. A. Petersson, H. Nakatsuji, M. Caricato, X. Li, H. P. Hratchian, A. F. Izmaylov, J. Bloino, G. Zheng, J. L. Sonnenberg, M. Hada, M. Ehara, K. Toyota, R. Fukuda, J. Hasegawa, M. Ishida, T. Nakajima, Y. Honda, O. Kitao, H. Nakai, T. Vreven, J. A. Jr. Montgomery, J. E. Peralta, F. Ogliaro, M. Bearpark, J. J. Heyd, E. Brothers, K. N. Kudin, V. N. Staroverov, R. Kobayashi, J. Normand, K. Raghavachari, A. Rendell, J. C. Burant, S. S. Iyengar, J. Tomasi, M. Cossi, N. Rega, J. M. Millam, M. Klene, J. E. Knox, J. B. Cross, V. Bakken, C. Adamo, J. Jaramillo, R. Gomperts, R. E. Stratmann, O. Yazyev, A. J. Austin, R. Cammi, C. Pomelli, J. W. Ochterski, R. L. Martin, K. Morokuma, V. G. Zakrzewski, G. A. Voth, P. Salvador, J. J. Dannenberg, S. Dapprich, A. D. Daniels, Ö. Farkas, J. B. Foresman, J. V. Ortiz, J. Cioslowski, D. J. Fox, Gaussian, Inc., Wallingford CT, (2009).
[27] S. Martinez, and I. Stern, Appl. Surf. Sci. 199 (2002) 83.
[28] N. M. Guan, L. Xueming, and L. Fei, Mat. Chem. Phy. 86 (2004) 59.
[29] S. S. Abd El Rehim, M. A. M. Ibrahim, and K. F. Khalid. Mat. Chem. Phy. 70 (2001) 268.
[30] M. Sahin, S. Bilgic, and H. Yilmaz, Appl. Surf. Sci. 195 (2002) 1.
[31] B. Ateya, B. E. El-Anadouli, and F. M. El-Nizamy, Corros. Sci. 24 (1984) 509.
[32] R. Solmaz, G. Kardas, M. Culha, B. Yazici, and M. Erbil, Electrochim. Acta 53 (2008) 5941.
[33] M. A. Migahed, and I. F. Nassar, Electrochim. Acta 53 (2008) 2877.
[34] A. Popova, M. Christov, S. Raicheva, and E. Sokolova, Corros. Sci. 46 (2004) 1333.
[35] F. Bentiss, M. Lebrini, M. Lagrenee, Corros. Sci. 47 (2005) 2915.
[36] J. B. Jorcin, M. E. Orazemb, N. Pébère, and B. Tribollet, Electrochim. Acta 51 (2006) 1473.

[37] F. Bentiss, B. Mernari, M. Traisnel, H. Vezin, and M. Lagrenée, Corros. Sci. 53 (2011) 487.
[38] K. R. Ansari, M. A. Quraishi, A. Singh, S. Ramkumar, and I. B. Obot, RSC Adv. 6 (2016) 24130.
[39] I. C. L. Valereto, S. Volynec, I. Ramires, A. C. Guastaldi, and I. Costa, J. Mater. Sci. Mater. Med. 15 (2004) 55.
[40] C. Verma, L. O. Olasunkanmi, E. E. Ebenso, M. A. Quraishi, and I. B. Obot, J. Phys. Chem. C 120 (2016) 11598.
[41] A. M. Amin, S. S. Abd, E. l. Rehim, and H. T. M. Abdel-Fatah, Corros. Sci. 51 (2009) 882−894.
[42] D. K. Yadav, B. Maiti, and M. A. Quraishi, Corros. Sci. 52 (2010) 3586.
[43] A. Dandia, S. L. Gupta, P. Singh, and M. A. Quraishi, Chem. Eng. 1 (2013)1303.
[44] M. A. Quraishi, A. Singh, V. K. Singh, D. K. Yadav, and A. K. Singh., Mater. Chem. Phys. 122 (2010) 114.
[45] D. K. Yadav, and M. A. Quraishi, Ind. Eng. Chem. Res. 51 (2012) 8194.
[46] I. B. Obot, D. D. Macdonald, and Z. M. Gasem, Corros. Sci. 99 (2015) 1.
[47] P. Geerlings, F. De Proft, and W. Langenaeker, Chem. Rev. 103 (2003) 1793.
[48] G. Gece, Corros. Sci. 50 (2008) 2981.
[49] M. A. Quraishi., and H. K. Sharma, Mater. Chem. Phys. 78 (2003) 18.
[50] E. E. Ebenso, D. A. Isabirye, and N. O. Eddy, Int. J. Mol. Sci. 11 (2010) 2473.
[51] F. Kandemirli, and S. Sagdinc, Corros. Sci. 49 (2007) 2118.
[52] N. V. Likhanova, M. A. D. Aguilar, O. O. Xometl, N. N. Entzana, E. Arce, and H. Dorantes, Corros. Sci. 52 (2010) 2088.
[53] R. G. Parr, and R. G. Pearson, J. Am. Chem. Soc. 105 (1983) 7512.
[54] R. G. Pearson, Inorg. Chem. 27 (1988) 734.
[55] V. S. Sastri, and J. R. Perumareddi, Corrosion 53 (1997) 617.
[56] R. G. Pearson, Proc. Nati. Acad. Sci. USA 83 (1986) 8440.
[57] P. K. Chattaraj, J. Phys. Chem. A 105 (2001) 511.
[58] X. Li, X. Xie, S. Deng, and G. Du, Corros. Sci. 92 (2015) 136.
[59] P. Mourya, P. Singh, A. K. Tewari, R. B. Rastogi, and M. M. Singh, Corros. Sci. 95 (2015) 71.
[60] B. Gómez, N. V. Likhanova, M. A. D. Aguilar, R. M. A. Palou, and J. L. Vela, J. Phys. Chem. B 110 (2006) 8928.
[61] A. G. Stoyanova Petkova, and S. D. Peyerimhoff, Chem. Phys. 279 (2002) 1.
[62] R. S. A. Hameed, E. A. Ismail, A. H. Abu-Nawwas, H. I. AL-Shafey, Int. J. Electrochem. Sci. 10 (2015) 2098.
[63] H. I. AL-Shafey, R. S. A. Hameed, F. A. Ali., A. A. S. Aboul-Magd, and M. Salah, Int. J. Pharm. Sci. Rev. Res. 27 (2014) 146.

[64] A. S. Fouda, M. S. Motawee, H. S. Megahid, and H. A. A. Mageed, Ind. J. Chem. Phram. Sci. 3 (2015) 1808.
[65] P. Geethamani, and P. K. Kasturi, J. Taiwan. Inst. Chem. Eng. 63 (2016) 490.
[66] R. S. A. Hameed, Port. Electrochim. Acta 29 (2011) 273.
[67] A.S. Fouda, W. M. Mahmoud, and H. A. A. Mageed, J. Bio. Tribo. Corros. 2 (2016) 7.
[68] P. Geethamani, P. K. Kasturi, and S. Aejitha, Elixir Corro. Dye. 76 (2014) 28406.
[69] R. S. A. Hameed, H. I. AL-Shafey, and A. H. Abu-Nawwas, Int. J. Electrochem. Sci. 9 (2014) 6006.